ISSN 2070-0482, Mathematical Models and Computer Simulations, 2023, Vol. 15, No. 3, pp. 415–426. © Pleiades Publishing, Ltd., 2023.
Russian Text © The Author(s), 2022, published in Matematicheskoe Modelirovanie, 2022, Vol. 34, No. 10, pp. 65–80.

Non-equilibrium Characteristics of Heat Transfer of Copper in a Wide Temperature Range

V. I. Mazhukin[a], O. N. Koroleva[a,*], M. M. Demin[a], and A. A. Aleksashkina[a]

[a] *Keldysh Institute of Applied Mathematics of RAS, Moscow, 125047 Russia*

**e-mail: koroleva.on@mail.ru*

Received August 5, 2022; revised September 1, 2022; accepted September 12, 2022

Abstract—The characteristics of nonequilibrium heat transfer of copper, such as thermal conductivity and heat capacity, are obtained in a wide temperature range ($300 \le T \le 5700$ K), including the region of melting-crystallization phase transformations by mathematical modeling. As is known, there are two mechanisms of heat transfer in a solid body: by elastic vibrations of the lattice and by free electrons. When determining these characteristics of copper heat transfer, the lattice and electronic components were taken into account. Modeling of the characteristics of heat transfer of the copper electronic subsystem in this work is based on the use of quantum statistics of the electron gas using the Fermi–Dirac integrals. The properties of the phonon subsystem were determined within the framework of the atomistic approach. The interaction potential of particles of the "embedded atom" family EAM was used for modeling. The simulation results were compared with the results of alternative calculations. The total heat capacity and thermal conductivity of copper, obtained by summing the electronic and phonon components, are compared with the experimental data.

Keywords: nonequilibrium copper heat transfer, electron gas quantum statistics, Fermi–Dirac integrals, molecular dynamics modeling

DOI: 10.1134/S2070048223030110

1. INTRODUCTION

The features of ultra-short laser action on metals and semiconductors put forward a number of problems for solving by means of mathematical modeling.

One of these problems is the quantitative assessment of the thermophysical characteristics of the phonon and electronic subsystems of metals. The interest in this problem was stimulated primarily by the need for a deeper understanding of the mechanisms of thermal conduction during nonequilibrium energy transfer in a number of applications [1–5].

The action of ultra-high-power ultra-short laser radiation on metals and semiconductors occurs over very short time and space scales, which leads to a violation of the general local thermodynamic equilibrium in them. The irradiated targets under these conditions are represented as two subsystems – electronic one and phonon one, each of which is in a state of local thermodynamic equilibrium, and is characterized by its own temperatures (electron T_e and phonon T_{ph} ones) and equations of state. As a consequence, all processes are described in the two-temperature approximation [6, 7]. A target under pico- and femtosecond action can be in the states with very high temperatures and pressures, in which the thermal and mechanical properties of the substance are not known at all. Therefore, the problem of determining the thermophysical, optical and thermodynamic characteristics for each of the subsystems in a wide (tens and hundreds of electron volts) temperature range is one of the most important problems for mathematical modeling. Modern description of properties in a wide temperature range, including the solid-liquid phase transition in metals, as well as in semiconductors, is carried out within the framework of two classes of models: continual [8–10] and atomistic [10–13] ones.

In this paper, the properties of the copper electronic subsystem are modeled using quantum statistics. The characteristics of the phonon subsystem of copper in the solid-liquid system are studied within the framework of the atomistic approach. The potential of the "embedded atom method" (EAM) developed and tested in [14] for copper was used as the interatomic interaction potential.

The purpose of this work is to determine the phonon, electronic and total thermal conductivity and heat capacity of copper in a wide temperature range ($300 \le T \le 5700$ K), including the region of the melting – crystallization phase transition.

The article presents the results of modeling, as well as the results of comparing the obtained characteristics of copper with experimental data and the results of alternative calculations, showing an acceptable qualitative and quantitative agreement.

2. MODELING OF THE CHARACTERISTICS OF HEAT TRANSFER OF THE ELECTRON SUBSYSTEM OF COPPER

The mentioned modeling in this work is based on the use of quantum statistics of the electron gas and Fermi-Dirac integrals. With this approach, the knowledge of the distribution law of the carriers over the energy states is the basis. The conduction electrons of copper can be considered as an ideal Fermi gas [15], which is degenerate at a temperature $T \ll T_F$ (T_F is the Fermi temperature). For a degenerate electron gas of metals, the distribution of carriers over energy states is subject to the Fermi-Dirac law

$$f_e = 1/\exp\left((\varepsilon_e - \mu(T_e))/(k_B T_e)\right) + 1, \tag{1}$$

where T_e, ε_e, are the electron temperature and energy, $\mu(T_e)$ is the chemical potential, $\mu(0) = \varepsilon_F$ is the Fermi energy. At $T > 0$, the Fermi energy has the meaning of the most probable or average energy of metal electrons that can take part in conduction at a given temperature. These electrons are responsible not only for creating electrical conductivity. It is they that determine the contribution of the electronic specific heat to the total specific heat of the crystal and to a large extent determine the thermal conductivity of the crystal. At $\varepsilon_e - \varepsilon_F \gg k_B T_e$, the degeneracy of the electron gas is removed, and the charge carriers obey the Maxwell-Boltzmann statistics

$$f_e \approx \exp\left((\varepsilon_F - \varepsilon_e)/(k_B T_e)\right). \tag{2}$$

2.1. Fermi-Dirac Integrals

For a quantitative description of the electrical, thermodynamic and thermophysical properties of a degenerate electron gas, the distribution function (1) and the Fermi-Dirac integrals are used

$$F_{k+1/2}(\eta(T_e)) = \int_0^\infty E_e^{k+1/2} dE_e \Big/ (\exp(E_e - \eta(T_e)) + 1), \tag{3}$$

where $E = \varepsilon_e / k_B T_e$, $\eta(T_e) = \mu(T_e)/k_B T_e$ are the dimensionless electron energy and chemical potential.

It is convenient to represent the Fermi integrals as functions of the dimensionless temperature $\xi = k_B T_e/\varepsilon_F$. In [16], for integrals of the form (3) at a constant electron density $N_e = \text{const}$, a convenient approximation was proposed that makes it possible to express the integrals $F_{k+1/2}(\xi)$ in terms of the transcendental Gamma functions $\Gamma(k + 1/2)$ and the dimensionless temperature ξ:

$$F_{k+1/2}(\xi) = A\xi^{-3/2}[1 + (B/\xi)^2]^{k/2}, \tag{4}$$

where $A = 2/3 \cdot \Gamma(k + 3/2)/\Gamma(3/2)$, $B = [A(k + 3/2)]^{-1/k}$ are the coefficients expressed in terms of Gamma function and which have the correct asymptotic for $\xi \to 0$ and $\xi \to \infty$.

$$F_{k+1/2}(\eta) \approx 1/\xi^{k+3/2}(k + 3/2), \quad \xi \to 0,$$
$$F_{k+1/2}(\eta) \approx \frac{2}{3}\frac{\Gamma(k + 3/2)}{\Gamma(3/2)}\frac{1}{\xi^{3/2}} \quad \xi \to \infty.$$

In this paper, Fermi-Dirac integrals are used for the values of $k = -1, 0, 1, 2$.

$$F_{-1/2}(\xi) = 4/3 \cdot \xi^{-1/2}\Big/(\xi^2 + 4/9)^{1/2}; \quad F_{1/2}(\xi) = 2/3 \cdot 1/\xi^{3/2};$$
$$F_{3/2}(\xi) = (\xi^2 + (2/5)^2)^{1/2}\Big/\xi^{5/2}; \quad F_{5/2}(\xi) = (5/2 \cdot \xi^{-3/2} + 2/7 \cdot \xi^{-7/2}). \tag{5}$$

2.2. Equations of State for Degenerate Electron Gas

Using expressions (5), the equations of state for a degenerate electron gas can be represented in the form of simple analytical expressions at arbitrary temperatures [8]. So the average energy of electrons $\langle \varepsilon_e \rangle$ and their pressure can be represented as

$$\langle \varepsilon_e \rangle = T_e \frac{F_{3/2}}{F_{1/2}} = \frac{3}{2}\varepsilon_F(\xi^2 + 0.16)^{1/2}, \tag{6}$$

$$p = \frac{2}{3} N_e \langle \varepsilon_e \rangle = \frac{2}{3} N_e T_e \frac{F_{3/2}}{F_{1/2}} = N_e \varepsilon_F(\xi^2 + 0.16)^{1/2}. \tag{7}$$

2.3. Heat Capacity of Electron Gas

Can be expressed as

$$C_e(T_e) = \frac{\partial}{\partial T}(N_e \langle \varepsilon_e \rangle). \tag{8}$$

Using the relations

$$\frac{\partial}{\partial \eta} F_{k+1/2} = (k + 1/2) F_{k-1/2} \quad \text{and} \quad \frac{\partial \eta}{\partial T} = \frac{3}{T}\frac{F_{1/2}}{F_{-1/2}},$$

One obtains from (8) the expression for the heat capacity of electron gas in terms of Fermi integrals:

$$C_e(T_e) = N_e/F_{1/2}(5/2F_{3/2} - 9/2F_{-1/2}), \tag{9}$$

where m is the electron mass, $\hbar$ is the Plank constant.

2.4. Thermal Conductivity Coefficient of Electron Gas $\kappa_e(T_e, T_{ph})$

According to the elementary kinetic theory [15], the thermal conductivity of the electron gas $\kappa_e(T_e, T_{ph})$ was determined through the heat capacity $C_e(T_e)$ and the averaged thermal diffusivity $\chi_{e,\,m}(T_e, T_{ph})$ of the electron gas of metals

$$\begin{aligned}\left(\kappa_e(T_e, T_{ph})\right)_k &= \left(1/3 \cdot C_e(T_e)\ell_e(T_e, T_{ph})\langle v_e \rangle\right)_k \\ &= \left(C_e(T_e)\chi_{e,m}(T_e, T_{ph})\right)_{k=s,\ell},\end{aligned} \tag{10}$$

where $\langle v_e \rangle$ is the average thermal velocity of electron, which is expressed in terms of its average energy $\langle \varepsilon_e \rangle$ (6)

$$\langle v_e \rangle = (2/m \cdot \langle \varepsilon_e \rangle)^{1/2}. \tag{11}$$

Thus, to obtain the thermal conductivity of the electron gas $\kappa_e(T_e, T_{ph})$, it is necessary to determine the thermal diffusivity of the electron Fermi gas $\chi_{e,\,m}(T_e, T_{ph})$.

2.4.1. Thermal diffusivity of an electron Fermi gas in the general case, the thermal diffusivity of electron Fermi gas is proportional to the product of the mean free path $\ell_e(T_e)$ and the mean electron velocity $\langle v_e \rangle$ (11):

$$\chi_e(T_e) = \frac{1}{3}\ell_e(T_e)\langle v_e \rangle, \, [\text{cm}^2/\text{s}].$$

In metals, the mean free path of electrons is determined by several mechanisms: paired electron-electron collisions, electron-phonon collisions, and scattering by plasmons. Pair electron-electron collisions dominate in the temperature range comparable to the Fermi energy $T_e/\varepsilon_F \sim 1$. Electron-phonon interaction dominates in the low temperature region, $T_e/\varepsilon_F \ll 1$. The interaction associated with the excitation of plasmons occurs at high temperatures exceeding the energy of the plasma frequency $T_e > \hbar\omega_r$ ($\hbar\omega_r \cong 10$–20 eV). Taking into account the high-temperature region of the occurrence and the limited experimental information on the decrease in the electron path due to the excitation of plasmons (it is known only for some metals), the scattering of electrons by plasmons is not considered.

In the nonequilibrium case, the thermal diffusivity of the metal $\chi_{e,\,m}(T_e,\,T_{ph})$ takes into account the electron-electron and electron-phonon interaction mechanisms and can be represented as:

$$\left(\chi_{e,m}(T_e,T_{ph})\right)_k = \left(\chi_{ee}(T_e)\chi_{eph}(T_e,T_{ph})\Big/\left(\chi_{ee}(T_e)+\chi_{eph}(T_e,T_{ph})\right)\right)_{k=s,\ell}, \tag{12}$$

where $\chi_{ee}(T_e)$, $\chi_{eph}(T_e,\,T_{ph})$ are the electron-electron and electron-phonon thermal diffusivity.

2.4.2. Electron-electron thermal diffusivity is proportional to the product of the electron mean free path in electron-electron collisions and the electron velocity

$$\chi_{ee}(T_e) = 1/3\cdot \ell_{ee}(T_e)\langle v_e\rangle. \tag{13}$$

According to the well-known gas-dynamic formula [17], the mean free path of an electron in pair electron-electron collisions $\ell_{ee}(T_e)$ is determined by $\ell_{ee}(T_e) = (1/N_e)\sigma_{ee}(T_e)$, where $\sigma_{ee}(T_e)$, where $\sigma_{ee}(T_e)$ is the scattering cross-section with energy transfer $\Delta\varepsilon$ for the electrons with energies ε_1, ε_2. The cross-section $\sigma_{ee}(T_e)$ is expressed in terms of the transport cross-section of the collision of two isolated electrons $\sigma_{ee}^{\rm tr}(T_e)$ and the Fermi integrals $F_{-1/2}$, $F_{1/2}$. The cross-sections σ_{ee} and $\sigma_{ee}^{\rm tr}$ are written as

$$\sigma_{ee}^{\rm tr} = 2\pi/9\cdot(4/9\pi)^{4/3} z^{-4/3}\cdot r^4/r_B^2\cdot\left(\ln(t+1)-t/(t+1)\right)\Big/(\xi^2+0.16),$$

$$\sigma_{ee} = \sigma_{ee}^{\rm tr}\left(F_{-1/2}/2F_{1/2}\right)^2,$$

where $t = 4\langle k\rangle^2 d^2 = (9\pi/4)^{4/3} z^{1/3}\cdot r_B/r\cdot[(\xi^2+0.16)\cdot(\xi^2+4/9)]^{1/2}$, $r_B = \hbar^2/me^2 = 0.529\times10^{-8}$ cm is the Bohr radius, $r = (3/4\pi N_a)^{1/3}$ is the average distance between atoms, e is the electron charge, $\langle k\rangle$ is the average wave vector of an electron, d is the Debye range of the field $U = e^2/r\cdot\exp(-r/d)$.

At low temperatures $T_e/\varepsilon_{\rm F} \ll 1$ the effective cross-section $\sigma_{ee}(T_e)$ is small and can be estimated as $\sigma_{ee}(T_e) = \sigma_{ee}^{\rm tr}(T_e)\xi^2/(\xi^2+4/9) \approx \sigma_{ee}^{\rm tr}(T_e)\cdot(T_e/\varepsilon_F)^2$. The maximum cross-section is reached at $T_e/\varepsilon_{\rm F} \geq 1$, when the degeneracy is removed and electron-electron collisions with a large energy transfer become possible. At very high temperatures $T_e/\varepsilon_{\rm F} \gg 1$, the cross-section becomes Coulomb and decreases according to the logarithmic law.

2.4.3. Electron-phonon thermal diffusivity $\chi_{eph}(T_e, T_{ph})$, determined by the electron-phonon interaction is described under the assumption of elastic scattering of metal conduction electrons by lattice vibrations

$$\left(\chi_{eph}(T_e,T_{ph})\right)_{k=s,\ell} = \left(\frac{1}{3}\ell_{eph}(T_{ph})\langle v_e(T_e)\rangle\right)_{k=s,\ell}, \tag{14}$$

where $(\ell_{eph})_{k=s,\ell} = (E\cdot r/zN_a k_{\rm B}T_{ph})_k$ [cm] is the mean free path determined by electron-phonon interaction, E is the Young's modulus, T_{ph} is the lattice temperature. The lower boundary of ℓ_{eph} is the Bohr diameter $d_{\rm B}$.

2.5. Calculation Results

The thermal conductivity and heat capacity of copper electron gas were obtained in the temperature range $300 \leq T \leq 5640$ K. Figure 1 shows the temperature dependence of the heat capacity of copper electron gas (9). The temperature dependence of the thermal conductivity of the electron gas of copper (10)-(14) is shown in Fig. 2.

In Figs. 1, 2, the vertical dotted lines indicate the equilibrium melting temperature $T_m = 1330$ K, which was obtained from molecular dynamics simulation in [12] with the potential [14], which was also used in this work to determine the properties of the phonon subsystem of copper. From the reference [18], the value of the equilibrium melting temperature obtained from MD modeling differs by $\Delta T_m = 1.96\%$. The error is quite acceptable for modeling.

At the equilibrium melting temperature T_m, the heat capacity of the electron gas of copper in the melt is greater than that in the crystal. The difference in heat capacity at the phase transition (Fig. 1) is insignificant and amounts to $\Delta C_e = (C_{e,\,\rm liq} - C_{e,\,\rm sol})/C_{e,\,\rm sol} = 0.18\%$. In contrast to the heat capacity, the thermal conductivity of the electron gas of copper at the melting–crystallization phase transition at $T = T_m$ decreases significantly (Fig. 2). The difference is $\Delta\kappa_e = (\kappa_{e,\,\rm sol} - \kappa_{e,\,\rm liq})/\kappa_{e,\,\rm sol} = 66.5\%$.

At Fig. 2, the marker shows the value of the electron thermal conductivity at $T = 300$ K from [19], which is obtained from the first principles, including density functional theory (DFT) to obtain the ther-

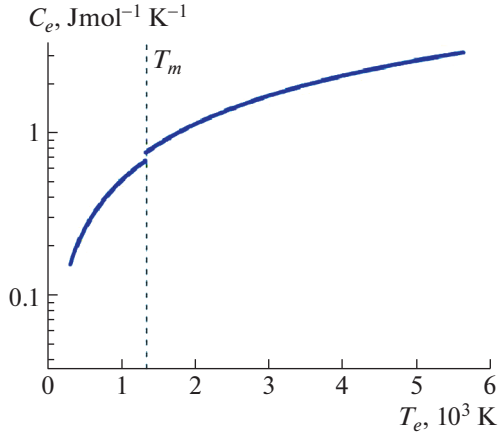

Fig. 1. Temperature dependence of the heat capacity of the copper electron gas.

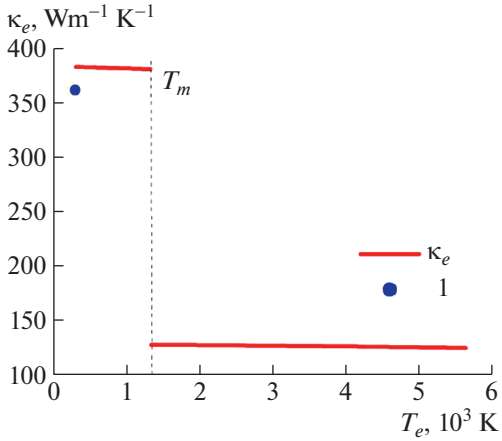

Fig. 2. Temperature dependence of the thermal conductivity of the copper electron gas κ_e. The markers (1) show the results of calculations [19].

mal transfer of phonons and electrons, taking into account electron-phonon and phonon-phonon scattering. At $T = 300$ K, the difference between the results is ~5.7%. The obtained temperature dependence of the electron thermal conductivity in the temperature range 300 K $\le T \le T_m$, as well as in the copper melt ($T_m \le T \le 5640$ K), is practically independent of temperature.

3. MODELING OF THE THERMAL TRANSFER CHARACTERISTICS OF THE PHONON SUBSYSTEM OF COPPER

Modeling of the characteristics of thermal transfer, heat capacity and thermal conductivity of the phonon subsystem of copper in this work is based on the atomistic approach. The atomistic models are based on the method of molecular dynamics (MD). The MD method is based on a model representation of a polyatomic molecular system, in which all atoms are represented by material points, and the motion is described in the classical case by Newton's equations. Because of this, atomistic models are a system of differential equations whose integration requires knowledge of the coordinates and velocities at the initial time $t = 0$ of all particles. The resulting system of ODEs is solved using the Verlet finite-difference scheme [20]. In the MD modeling of the properties of copper, the semiempirical potential of the "embedded atom method" (EAM), developed and tested for copper in [14], was used as the interparticle interaction potential. The temperature and pressure are controlled by a thermostat and a Berendsen barostat [21]. The

experiments were carried out using the LAMMPS package [22], which is a simulator for atomic and molecular modeling.

3.1. Thermal Conductivity of Phonon Subsystem of Copper

Was determined from MD simulation by the direct method (DM) [23] in the range $300 \le T \le 5700$ K. More details on the use of DM to determine the thermal conductivity are presented in [24, 25]. The initial size of the region for obtaining the phonon thermal conductivity of copper was $10 \times 10 \times 20$ unit cells (lattice constant 0.361 nm), which corresponds to 8000 particles. Periodic boundary conditions were set along three axes. The sample along the x axis was divided into the number of cells corresponding to the number of particles. At each time step, a fixed amount of heat δQ_N was put into the heating region, and the same amount was taken from the sink region. The heat flux W was calculated as

$$W = dQ/(SNdt)/2, \tag{15}$$

where $dQ = N \times dt \times \delta Q_N$ is the total deposited energy, δQ_N is the energy deposited during 1 time step, N is the number of steps, dt is the size of time step, S is the domain cross-section. The choice of the time step depended on temperature and was from 3 fs at 300 K to 1 fs at 4000 K and above. Division by 2 is used because of periodic boundary conditions, i.e. heat spreads in 2 directions. The resulting temperature gradient is then calculated. The thermal conductivity coefficient κ_{ph} was determined by the direct nonequilibrium method from the known heat flux from the Fourier law

$$W = -\kappa_{ph}\partial T/\partial x, \tag{16}$$

where W is the heat flux, x is the coordinate in the direction of the flux.

According to the direct nonequilibrium method, to obtain a constant heat flux, it is necessary that the size of the simulation cell be much larger than the phonon mean free path, which leads to the consideration of large samples. This is the difficulty in applying the direct method to solids, since, in calculations with a small number of atoms, the thermal conductivity coefficient turns out to be dependent on the length of the region due to phonon scattering at the boundary. To overcome the effects of a finite size, a scaling procedure was carried out, which consists in the following: for each temperature value, the inverse dependence of the thermal conductivity $1/\kappa_{ph}$ was constructed with respect to the reciprocal of the length of the computational domain L_n, $1/L_n$, from which the thermal conductivity was determined by extrapolating the data $1/L_n \to 0$ [23].

The heat flux was determined from the results of a series of calculations. The number of computational regions and their sizes depended on the temperature for which the thermal conductivity was calculated. The lower the temperature, the more regions were selected. For the range $300 \le T \le 900$ K, the calculations were performed for 8 regions of different sizes L_n of unit cells corresponding to the number of particles. For the range $1200 \le T \le 2000$ K, three calculations were performed for three region sizes L_n, and for $T \ge 4000$ K, only one calculation was performed. The cross-section of the region was constant: $S = 10 \times 10$ cells. The heat flux was determined from the temperature difference between the areas of heating and heat sink, for which the instantaneous temperature difference was averaged over the entire calculation time after the establishment of a stationary distribution. To improve the accuracy of calculations, the temperature difference was calculated not over the entire interval between the source and sink, but over its central part (0.8 of the total length) (Fig. 3).

After a series of calculations for each temperature from the range $300 < T < 5700$ K, the scaling procedure was carried out and the thermal conductivity was calculated. For example, the determination of thermal conductivity for $T = 300$ K was carried out according to the results of calculations for the 5 largest lengths of the computational region. Using the least squares method [26], the corresponding five values of the inverse thermal conductivity were approximated by the linear dependence

$$P(z) = 0.081 + 8.988z, \tag{17}$$

where $z = 1/L_n$ ($n = 1, 2, 3, 4, 5$).

The approximation error, according to the least squares criterion [26], was $\Delta = 0.004$ $(\text{W/mK})^{-1}$. At $z = 1/L_n = 0$, we obtain the value $P(0) = 0.081$, the inverse of which will be equal to the thermal conductivity coefficient for a given temperature (300 K). At the temperature of 300 K, the phonon thermal conductivity is $\kappa_{ph}(T = 300\text{ K}) = 12.408$ W/mK, which corresponds to an infinite region length L_n. At Fig. 4, the linear dependence (17) is shown by a red line with markers. The procedure was repeated for all required temperatures in the range $300 \le T \le 5700$ K.

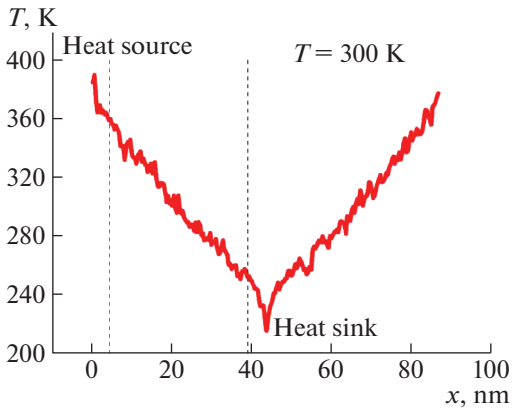

Fig. 3. Spatial temperature profile at one moment in time. The dotted lines mark the interval in which the temperature gradient was measured.

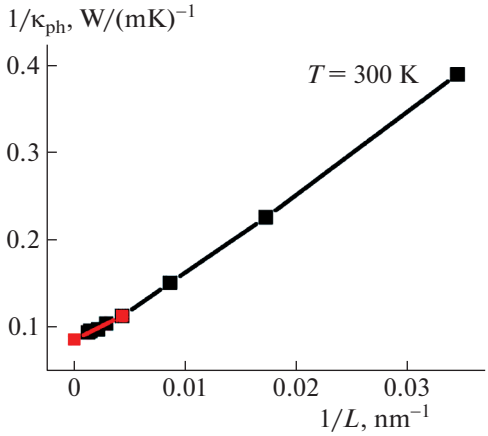

Fig. 4. Dependence of the reciprocal value of thermal conductivity on the reciprocal value of the region size for the temperature $T = 300$ K.

The results of calculating the thermal conductivity of copper are shown at Fig. 5. The inset of Fig. 5 shows the temperature dependence of the thermal conductivity of copper at the solid-liquid phase transition.

At the equilibrium melting temperature $T_m = 1330$ K, the thermal conductivity abruptly decreases. In the solid phase at $T_m = 1330$ K, the thermal conductivity is $\kappa_{ph} = 1.55$ W/mK, while in the melt at the same temperature, the thermal conductivity is $\kappa_{ph} = 1.29$ W/mK. The difference between the solid and liquid phases, clearly visible in the inset of Fig. 5, is 16.77%. The calculation was carried out up to a temperature $T = 5700$ K, at which the thermal conductivity is $\kappa_{ph} = 0.647$ W/mK. The markers in Fig. 5 show the results of calculations of the phonon thermal conductivity in [27] in the range $300 \le T \le 1000$ K, obtained by first-principles calculations with allowance for phonon-phonon and electron-phonon scattering, using the density functional theory (DFT) with an exchange-correlation functional of the type generalized gradient approximation (GGA). As we can see, there is good agreement with the results of [27].

3.2. Heat Capacity of the Phonon Subsystem of Copper

The temperature dependence of the lattice heat capacity $C_{ph}(T)$ in the temperature range $300 < T < 5800$ K at constant pressure P was determined in this work from the values of the enthalpy $H(T)$ obtained in the course of a computational MD experiment.

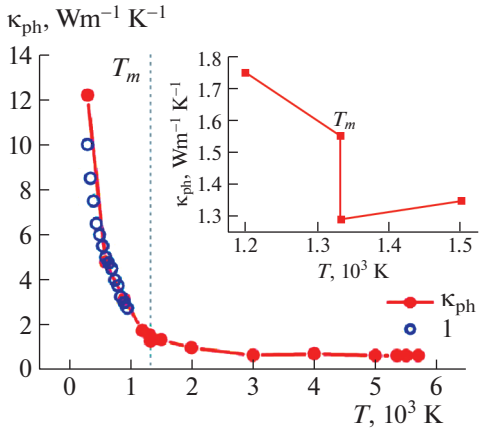

Fig. 5. Temperature dependence of the phonon thermal conductivity of copper κ_{ph}. (1) results of calculations from [27]. On the inset—in enlarged form, the temperature dependence of the phonon thermal conductivity of copper at the solid-liquid phase transition.

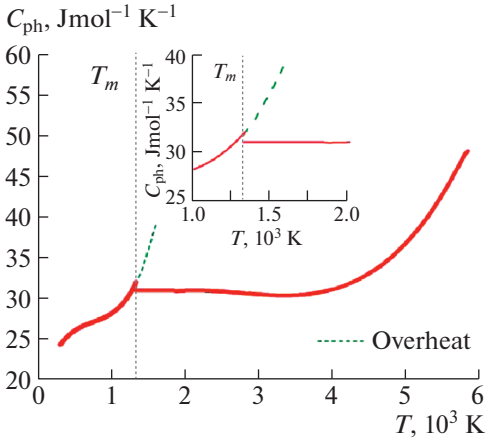

Fig. 6. Temperature dependence of the phonon heat capacity of copper. The dotted line shows the overheating of the solid phase of copper in the temperature range $T_m < T < 1.2T_m$.

The values of $H(T)$ were approximated for the liquid and solid phases by polynomials $\tilde{H}(T)$. The temperature dependence of the heat capacity $C_{ph}(T)$ for each phase was determined by differentiating the corresponding dependence $\tilde{H}(T)$:

$$C_{ph}(T) = \left(\partial \tilde{H}(T)/\partial T\right)_P. \tag{17}$$

The temperature dependence of the phonon heat capacity $C_{ph}(T)$ of copper is shown at Fig. 6. The inset of Fig. 6 shows, in an enlarged form, the temperature dependence of the phonon heat capacity in the region of the solid-liquid phase transition.

At the equilibrium melting temperature T_m (Fig. 6), an insignificant, amounting to ~3.128%, abrupt decrease in the heat capacity of copper occurs, which is clearly visible in the inset of Fig. 6. On the inset of Fig. 6, the increase in the heat capacity to $C_{ph}(T) \approx 39$ J mol^{-1} K^{-1} is also clearly visible. It occurs when the solid phase is overheated in the temperature range $T_m < T < 1.2T_m$, shown by the dotted line. As the temperature increases $T_m < T < 2.63T_m$, the value of the heat capacity in the melt is almost constant and amounts to $C_{ph}(T) \approx 31.0$ J mol^{-1} K^{-1}. At a temperature $T > 4000$ K, the heat capacity of copper increases. At $T = 5800$ K its value is $C_{ph}(T) = 47.698$ J mol^{-1} K^{-1}.

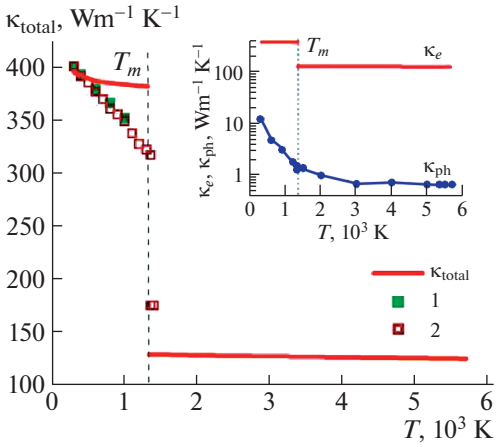

Fig. 7. Temperature dependence of total thermal conductivity $\kappa_{total}(T)$ of copper at $T = T_e = T_{ph}$. Markers are experimental data (1) [18], (2) [29]. In the inset, the temperature dependences of the electronic κ_e and phonon κ_{ph} thermal conductivity of copper.

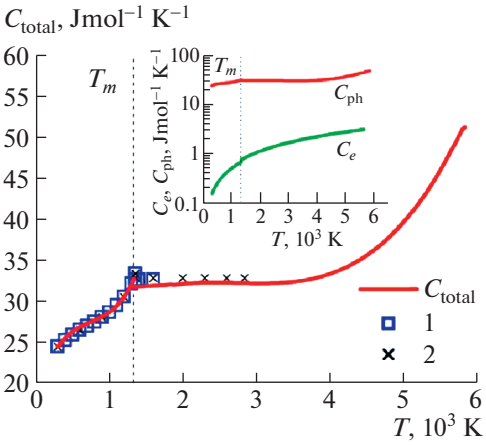

Fig. 8. Temperature dependence of the total heat capacity of copper $C_{total}(T)$ at $T = T_e = T_{ph}$. Markers are experimental data (1) [18], (2) [28]. The inset shows the temperature dependences of the electronic C_e and phonon C_{ph} heat capacities of copper.

4. TOTAL HEAT CAPACITY AND HEAT CONDUCTIVITY OF COPPER

The transfer of thermal energy in a solid is carried out by free charge carriers and phonons; therefore, the total heat capacity $C(T_e, T_{ph})$, as well as the total thermal conductivity $\kappa(T_e, T_{ph})$, are determined by the electronic and phonon components. Under conditions of thermodynamic equilibrium $T = T_e = T_{ph}$, the total (common) heat capacity and thermal conductivity can be represented as

$$C(T_e, T_{ph}) = C_e(T_e) + C_{ph}(T_{ph}), \quad \kappa(T_e, T_{ph}) = \kappa_e(T_e, T_{ph}) + \kappa_{ph}(T_{ph}).$$

The temperature dependences of the total heat capacity and thermal conductivity are shown at Figs. 7, 8. The markers at these figures show the reference values of the total heat capacity and thermal conductivity [18, 28, 29]. The insets of Figs. 7 and 8 show the temperature dependences of the thermal conductivity κ_e, κ_{ph} and the heat capacity C_e, C_{ph} of the electron and phonon gas.

Figures 9, 10 show the temperature dependences of the contribution of the phonon thermal conductivity (Fig. 9) and heat capacity (Fig. 10) of copper to the total thermal conductivity and heat capacity. The insets in these figures show the contributions of the electronic components to the overall values.

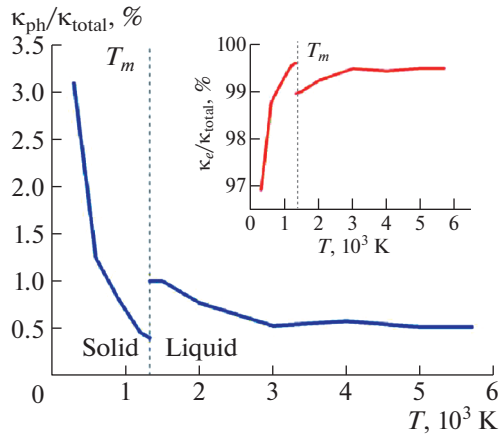

Fig. 9. Temperature dependence of the contribution of the phonon thermal conductivity of copper to the total one.

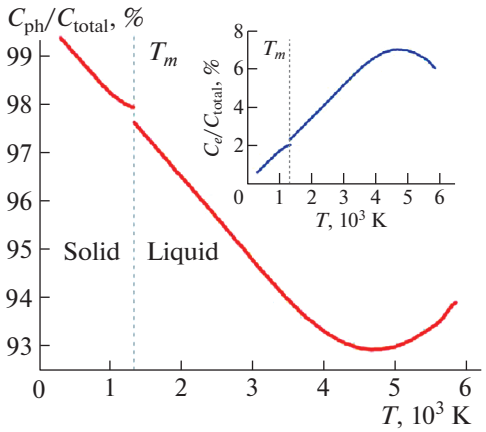

Fig. 10. Temperature dependence of the contribution of the phonon heat capacity of copper to the total one.

It can be seen that the decisive contribution to the total thermal conductivity of copper (Figs. 7, 9) is made by the electronic component κ_e, while the contribution of the phonon component κ_{ph} is small. At $T = T_{ph} = T_e = 300$ K, the contribution of $\kappa_e(T_e, T_{ph})$ to the total value is ≈97%, in the melt >99% (Fig. 9). According to [19], the contribution of the electronic component to the total thermal conductivity is ≈95%. The result obtained is consistent with the alternative estimate. As we can see, in the total thermal conductivity of copper (in the solid and liquid phases), the contribution of the electronic component is decisive.

An opposite situation is observed for the total heat capacity of copper (Fig. 8). The contribution of the phonon component to the total specific heat capacity of copper is decisive. At $T = 300$ K, the contribution of $C_{ph}(T_{ph})$ is more than 99%. Accordingly, the contribution of the electronic component $C_e(T_e)$ at $T_{ph} = T_e = 300$ K is less than 1% (Figs. 8, 10).

With increasing temperature, the contribution of the electronic heat capacity $C_e(T)$ somewhat increases and at $T = 4500$ K it is ~7%. However, the contribution of $C_{ph}(T)$ still remains dominant, which at $T = 4500$ K is ~93% (Fig. 10).

At Figs. 7 and 8, the markers show the reference values of the total thermal conductivity and heat capacity [18, 28, 29].

The total thermal conductivity obtained in this work at $T = T_e = T_{ph} = 300$ K differs minimally from the reference values [18, 29] by ~1.5%. The difference increases with increasing temperature. At $T = T_m$ in the solid phase, the reference value [29] is less than that obtained in this work by ~15.7%. At the same

temperature in the melt, the reference value [29] of thermal conductivity is higher than the calculated value by ~35.96%.

A comparison of the reference [28, 29] and calculated values of the total heat capacity of copper shows complete agreement in the solid phase in the temperature range 300 K $\le T \le T_{\text{m}}$. And almost complete agreement in the melt $T \ge T_{\text{m}}$, the deviation is ~2%.

Thus, we observe a good agreement between the obtained values of the heat capacity and thermal conductivity of copper and the reference data [18, 28, 29].

CONCLUSION

Using the methods of mathematical modeling, the characteristics of nonequilibrium heat transfer of copper, thermal conductivity and heat capacity, are obtained in a wide temperature range ($300 \le T \le 5700$ K), including the melting-crystallization phase transformation region. When determining the characteristics of heat transfer, the electronic and phonon components were taken into account. The values of the total equilibrium heat capacity and thermal conductivity were calculated for $T = T_e = T_{ph}$.

The heat capacity of copper at $T > 300$ K is mainly determined by lattice vibrations. The contribution of the phonon component to the heat capacity is $C_{ph}(T_{ph}) > 99\%$, and that of the electron component is $C_e(T_e) < 1\%$. With increasing temperature, the contribution of $C_{ph}(T_{ph})$ decreases and at $T = 4500$ K it is 93% (Fig. 9); accordingly, the contribution of the electronic component increases to 7%.

In contrast to the heat capacity, the contribution of the electronic component to the thermal conductivity of copper is significant. In the temperature range 300 K $\le T \le T_m$, according to the simulation results, $\kappa_e(T_e, T_{ph})$ of copper is ≈97%, in the liquid phase at $T \ge T_m$, it is more than 99% (Fig. 10). Correspondingly, the contribution of the phonon component $\kappa_{ph}(T_e, T_{ph})$ to the total thermal conductivity $\kappa_{ph}(T)$ decreases from 3% at $T = 300$ K to 0.5% at $T = 5000$ K.

ACKNOWLEDGMENTS

The work was supported by Russian Science Foundation, project no. 18-11-00318.

The results were obtained using the equipment of Shared Resource Center of KIAM RAS (http://ckp.kiam.ru).

CONFLICT OF INTEREST

The authors declare that they have no conflicts of interest.

REFERENCES

1. A. V. Mazhukin, V. I. Mazhukin, and M. M. Demin, "Modeling of femtosecond laser ablation of Al film by laser pulses," Appl. Surf. Sci. **257** (12), 5443–5446 (2011). https://doi.org/10.1016/j.apsusc.2010.11.154
2. R. Venkatasubramanian, E. Siivola, T. Colpitts, and B. O. Quinn, "Thin-film thermoelectric devices with high room-temperature figures of merit," Nature **413**, 597–602 (2001). https://doi.org/10.1038/35098012
3. E. G. Gamaly, *Femtosecond Laser-Matter Interaction*: *Theory, Experiments and Applications* (Jenny Stanford, New York, 2011).
4. E. G. Gamaly, *Femtosecond Laser-Matter Interactions*: *Solid-Plasma-Solid Transformations at the Extreme Energy Density*, 2nd ed. (Jenny Stanford, Singapore, 2022).
5. G. M. Petrov, A. Davidson, D. Gordon, and J. Peñano, "Modeling of short-pulse laser-metal interactions in the Warm Dense Matter regime using the two-temperature model," Phys. Rev. E **103** (3), 033204 (2021). https://doi.org/10.1103/PhysRevE.103.033204
6. V. I. Mazhukin, M. M. Demin, A. V. Shapranov, and A. V. Mazhukin, "Role of electron pressure in the problem of femtosecond laser action on metals," Appl. Surf. Sci. **530**, 147227 (2020). https://doi.org/10.1016/j.apsusc.2020.147227
7. M. I. Kaganov, I. M. Lifshitz, and L. V. Tanatarov, "Relaxation between electrons and the crystalline lattice," Sov. Phys. JETP **4** (2), 173–178 (1957).
8. V. I. Mazhukin, "Kinetics and dynamics of phase transformations in metals under action of ultra-short high-power laser pulses," in *Laser Pulses – Theory, Technology, and Applications*, Ed. by I. Peshko (IntechOpen, Rijeka, Croatia, 2012), Chapter 8, pp. 219–276. https://doi.org/10.5772/50731

9. A. V. Mazhukin, O. N. Koroleva, V. I. Mazhukin, and A. V. Shapranov, "Continual and molecular dynamics approaches in determining thermal properties of silicon," Proc. SPIE **10453**, 104530Y (2017). https://doi.org/10.1117/12.2271999
10. P. A. Loboda, N. A. Smirnov, A. A. Shadrin, and N. G. Karlykhanov, "Simulation of absorption of femtosecond laser pulses in solid-density copper," High Energy Density Phys. **7** (4), 361–370 (2011). https://doi.org/10.1016/j.hedp.2011.06.007
11. V. I. Mazhukin, O. N. Koroleva, A. V. Shapranov, M. M. Demin, and A. A. Aleksashkina, "Determination of thermal properties of gold in the region of melting–crystallization phase transition: Molecular dynamics approach," Math. Models Comput. Simul. **14** (4), 662–676 (2022). https://doi.org/10.1134/S2070048222040068
12. V. I. Mazhukin, M. M. Demin, and A. A. Aleksashkina, "Atomistic modeling of thermophysical properties of copper in the region of the melting point," Math. Montis. **XLI**, 99–111 (2018).
13. D. P. Sellan, E. S. Landry, J. E. Turney, A. J. H. McGaughey, and C. H. Amon, "Size effects in molecular dynamics thermal conductivity predictions," Phys. Rev. B **81** (21), 214305 (2010). https://doi.org/10.1103/PhysRevB.81.214305
14. Y. Mishin, M. J. Mehl, D. A. Papaconstantopoulos, A. F. Voter, and J. D. Kress, "Structural stability and lattice defects in copper: *Ab initio*, tight-binding, and embedded-atom calculations," Phys. Rev. B **63** (22), 224106 (2001). https://doi.org/10.1103/PhysRevB.63.224106
15. N. W. Ashcroft and N. D. Mermin, *Solid State Physics* (Saunders College, Philadelphia, 1976).
16. Yu. V. Martynenko and Yu. N. Yavlinskii, "Cooling of the electron gas of a metal at high temperatures," Sov. Phys. Dokl. **28**, 391–392 (1983).
17. D. V. Sivukhin, *General Course of Physics*. Vol. II: *Thermodynamics and Molecular Physics* (Fizmatlit, Moscow, 2005) [in Russian].
18. I. S. Grigoriev and E. Z. Melikhov (eds.), *Physical Quantities*: *Handbook* (Energoatomizdat, Moscow, 1991) [in Russian].
19. Z. Tong, S. Li, X. Ruan, and H. Bao, "Comprehensive first-principles analysis of phonon thermal conductivity and electron-phonon coupling in different metals," Phys. Rev. B **100** (14), 144306 (2019). https://doi.org/10.1103/PhysRevB.100.144306
20. L. Verlet, "Computer "Experiments" on Classical Fluids. I. Thermodynamical Properties of Lennard-Jones Molecules," Phys. Rev. **159** (1), 98–103 (1967). https://doi.org/10.1103/PhysRev.159.98
21. H. J. C. Berendsen, J. P. M. Postma, W. F. van Gunsteren, A. DiNola, and J. R. Haak, "Molecular dynamics with coupling to an external bath," J. Chem. Phys. **81** (8), 3684–3690 (1984). https://doi.org/10.1063/1.448118
22. S. Plimpton, "Fast parallel algorithms for short-range molecular dynamics," J. Comput. Phys. **117** (1), 1–19 (1995). https://doi.org/10.1006/jcph.1995.1039
23. L. Hu, W. J. Evans, and P. Keblinski, "One-dimensional phonon effects in direct molecular dynamics method for thermal conductivity determination," J. Appl. Phys. **110** (11), 113511 (2011). https://doi.org/10.1063/1.3660234
24. O. N. Koroleva, M. M. Demin, A. V. Mazhukin, and V. I. Mazhukin, "Modeling of electronic and phonon thermal conductivity of silicon in a wide temperature range," J. Phys.: Conf. Ser. **1787**, 012026 (2021). https://doi.org/10.1088/1742-6596/1787/1/012026
25. A. A. Aleksashkina, M. M. Demin, and V. I. Mazhukin, "Molecular dynamic calculation of lattice thermal conductivity of gold in the melting-crystallization region," Math. Montis. **XLVI**, 106–122 (2019). https://doi.org/10.20948/mathmontis-2019-46-9
26. A. A. Samarskii and A. V. Gulin, *Numerical Methods* (Nauka, Moscow, 1992) [in Russian].
27. Y. Wang, Z. Lu, and X. Ruan, "First principles calculation of lattice thermal conductivity of metals considering phonon-phonon and phonon-electron scattering," J. Appl. Phys. **119** (22), 225109 (2016). https://doi.org/10.1063/1.4953366
28. M. W. Chase, Jr., C. A. Davies, J. R. Downey, Jr., D. J. Frurip, R. A. McDonald, and A. N. Syverud (Eds.), "JANAF Thermochemical Tables, Third edition," J. Phys. Chem. Ref. Data **14** (Suppl. 1), 1–1856 (1985).
29. V. E. Zinov'ev, *Thermophysical Properties of Metals at High Temperatures* (Metallurgiya, Moscow, 1989) [in Russian].

SPELL: OK